Journal of Materials Chemistry A

Asymmetric electrode ionomer for low relative humidity operation of anion exchange membrane fuel cells

Journal:	*Journal of Materials Chemistry A*
Manuscript ID	TA-ART-06-2020-005807
Article Type:	Paper
Date Submitted by the Author:	10-Jun-2020

Complete List of Authors:	Leonardo, Daniel; Los Alamos National Laboratory, MPA-11 Maurya, Sandip; Los Alamos National Laboratory, MPA-11: Materials Synthesis and Integrated Devices Park, Eun Joo; Los Alamos National Laboratory, Delfin Manriquez, Luis; Los Alamos National Laboratory Noh, Sangtaik; Rensselaer Polytechnic Institute, Wang, Xiafeng; Rensselaer Polytechnic Institute, Bae, Chulsung; Rensselaer Polytechnic Institute, Chemistry and Chemical Biology Baca, Ehren; Sandia National Laboratories Fujimoto, Cy; Sandia National Laboratories , Organic Materials Kim, Yu Seung; Los Alamos National Laboratory,

ARTICLE

Received 00th January 20xx,
Accepted 00th January 20xx
DOI: 10.1039/x0xx00000x

Asymmetric electrode ionomer for low relative humidity operation of anion exchange membrane fuel cells

Daniel P. Leonard,[a] Sandip Maurya,[a] Eun Joo Park,[a] Luis Delfin Manriquez,[a] Sangtaik Noh,[b] Xiaofeng Wang,[b] Chulsung Bae,*[b] Ehren Donel Baca,[c] Cy Fujimoto,[c] and Yu Seung Kim*[a]

The operation of fuel cells under low relative humidity (RH) conditions gives substantial cost and performance benefits. Nonetheless, it is not currently feasible to operate anion exchange membrane fuel cells (AEMFCs) at low RH conditions because current materials for membrane electrode assembly cannot provide sufficient water for oxygen reduction reaction under low RH conditions. Here we synthesized polyfluorene ionomers with different ammonium concentrations for anode and cathode to control water management. We designed several asymmetric electrodes that enable high performance under low RH conditions via not only conventional backward water diffusion (anode to cathode) but also forward diffusion (cathode to anode). The AEMFCs using optimized asymmetric electrodes exhibited high H_2/CO_2-free air performance rated power density of circa 540 mW cm^{-2} at 90°C under 75% (anode) and 50% RH (cathode) conditions, which is comparable to those of state-of-the-art AEMFCs under nearly water-saturated conditions. The durability of the AEMFCs is excellent, generating 0.6 A cm^{-2} for > 900 h at 80°C under 50% RH (cathode) conditions. This study demonstrates that high-performance and durable AEMFCs under low RH and high current generating conditions are possible.

Introduction

Over the last decade, significant research progress has been made in the performance of anion exchange membrane fuel cells (AEMFCs). Several polyolefinic and polyaromatic membranes and ionomers enable power densities > 1,500 mW cm^{-2} under H_2/O_2 conditions and ca. 1,000 mW cm^{-2} under H_2/air conditions have been developed.[1-6] AEMFC's performance using platinum group metal-free (PGM-free) oxygen reduction reaction (ORR) catalysts reached > 900 mW cm^2 under H_2/O_2 conditions.[7-9] Low PGM loading hydrogen oxidation reduction (HOR) catalysts (≤ 0.1 mg_{Pt} cm^{-2}),[10, 11] or PGM-free HOR catalysts[12, 13] have also been developed, although the AEMFC performance using these catalysts needs further improvement.

Some remaining performance challenges for commercial viability of AEMFCs include operating AEMFCs under hot and reduced relative humidity (RH) conditions.[14] The advantage of low RH operation is apparent at the stack level in which low humidity operation reduces the required humidification capacity. Such conditions are particularly desirable for automotive applications in which the size of the radiator and humidifier is a critical cost factor for an efficient fuel cell system.[15] While current proton exchange membrane fuel cells demonstrate excellent performance at 80–100 °C and inlet RH of ca. 65%,[16] operating AEMFCs under such conditions is challenging. Unlike proton exchange membrane fuel cells, where water is simply a by-product of ORR, in AEMFCs, water is both a product of HOR and reactant of ORR. As such, a delicate water balance between anode and cathode is required. Currently-available polymer electrolytes cannot supply enough water for ORR under reduced RH conditions.

The stability of polymer electrolytes is another critical factor related to fuel cell operation at high temperatures and reduced RHs. Some researchers have reported that the stability of cationic functional groups, quaternized polymers, and AEMFCs are significantly reduced as the temperature increases to ≥ 80 °C.[7, 17, 18] Other researchers have reported that the alkaline stability of quaternized polymers is further reduced under low humidity[19-21] and high current generating conditions.[22, 23] In AEMFC, water is electrochemically generated at the anode and consumed at the cathode during cell operation. Additionally, water moves from the cathode to the anode by electro-osmotic drag. Therefore, the AEMFC cathode is prone to dry out during high current density operation in which degradation of the cathode ionomeric binder can be accelerated. High RH dependency of hydrocarbon-based quaternized polymers increases the difficulty of fuel cell operation at high temperatures and reduced RHs. Because the hydroxide conductivity of quaternized polymers strongly depends on hydration,[24] low cell resistance and high electrocatalytic reaction rates of AEMFCs are attained only when the membrane and ionomeric binders are sufficiently hydrated. Due to this fact, the relatively high water content in the electrodes is required for high performance to provide a significant amount of water to the membrane.[25-27] For these reasons mentioned above, all high-performance AEMFCs reported in the literature (H_2/O_2 power density > 1,000 mW cm^{-2}) were obtained under nearly water-saturated conditions. Earlier attempts to reduce reactant gas dew points using commercial Tokuyama ionomer (AS-4) produced low H_2/O_2 AEMFC performance (power density < 500 mW cm^{-2})[28, 29], and the durability of the cell was questionable.

[a] MPA-11: Materials Synthesis & Integrated Devices, Los Alamos National Laboratory, Los Alamos, New Mexico 87545, USA. E-mail: yskim@lanl.gov
[b] Department of Chemistry and Chemical Biology, Rensselaer Polytechnic Institute, Troy, New York 12180, USA. E-mail: baec@rpi.edu
[c] Materials Science and Engineering Center, Sandia National Laboratories, Albuquerque, New Mexico 87185, USA.

Here we demonstrate high-performance and durable AEMFC membrane electrode assemblies (MEAs) under high temperature and reduced RH conditions for the first time. We designed MEAs with two different ionomers for anode and cathode (asymmetric electrode ionomer) to control water management for high temperature and low RH operation of AEMFCs. For operation at high temperature, ca. ≥ 80 °C, we chose thermo-oxidative and alkaline-stable hexyltrimethyl ammonium-functionalized Diels-Alder poly(phenylene) AEM (HTMA-DAPP, **Fig. 1a**).[18, 30, 31] We chose the quaternized poly(fluorene) ionomer (FLNs) for the ionomeric binder (**Fig. 1b**). FLNs are known to have minimal phenyl adsorption on electrocatalysts because the phenyl group in the fluorene moiety has the lowest phenyl adsorption energy on Pt, ca. -1.38 eV compared to those of phenyl groups in other polyaromatics (ranged from -1.52 to -3.94 eV).[32] The low phenyl adsorption energy not only improves the HOR activity of Pt-based catalysts,[33] but also reduces the phenyl oxidation at the cathode.[34] We synthesized two FLN ionomers with different ion exchange capacities (IEC), ca. 2.5 and 3.5 mequiv. g^{-1}. The FLN with lower IEC (FLN-55) showed one of the best AEMFC performance and durability under fully hydrated conditions.[35] We used the FLN with the higher IEC (FLN-100) along with FLN-55 for asymmetric electrode MEAs in this study.

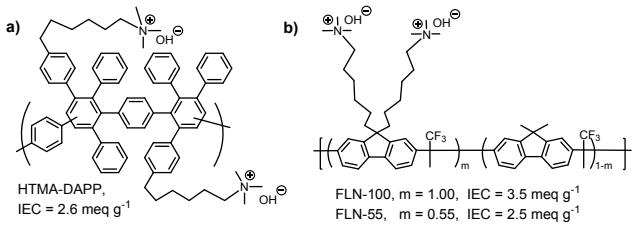

Fig. 1 The chemical structure of (a) HTMA-DAPP AEM and (b) FLN ionomeric binder used in this study.

Results and Discussion

Synthesis and properties of FLNs

We have synthesized FLNs via one-pot, acid-catalysed Friedel-Crafts polycondensations of 1,1,1-trifluoroacetone and fluorene monomers and subsequent amination with trimethylamine.[35] The IEC values of the polymers were measured by ^{1}H NMR spectroscopies by comparing the integral ratio of the peak at 3.22 ppm (from the –CH_2Br peak of 9,9-bis(6-bromoheyl)fluorene) and the peak at 2.01 ppm (from the –CF_3CCH_3- of the backbone) of the precursor polymer.[35] The alkaline stability of FLNs was excellent; no chemical structural changes by ^{1}H NMR were observed with the polymers after immersing the polymer for 30 days in 1 M NaOH at 80°C.[35]

The hydroxide conductivity and hydrophilicity of the ionomeric binder play critical roles in low RH AEMFC operation. Because FLN-100 has a high IEC, the mechanical properties of the cast membrane are too low to measure the stand-alone film conductivity (note that the film formation ability is not a critical requirement for the ionomeric binder in the catalyst layer). Due to the difficulty of the film conductivity measurement, we measured the solution conductivity of FLNs as a function of water content using dimethylsulfoxide (DMSO)/water solvent mixtures to estimate hydroxide condutivity. FLN-55 was not homogeneously dissolved when water content content of the solvent exceeded 50%. However, the solutions with less than 50% water showed a linear relationship between water content and hydroxide conductivity, thus conductivity at full hydradtion could be extrapolated. The conductivity values reported here likely do not reflect the true hydroxide conductivity value of the ionomer film. However, they do show a clear trend relating level of hydration with solution conductivity. **Fig. 2** compares the hydroxide conductivity of the FLN-55 and FLN-100 solutions (5 wt.%) as a function of water content. The hydroxide conductivity of two FLN ionomer solutions increases as water content in the solution increases (**Fig. 2a**). This is expected as dielectric constant of the mixture increases from 47.0 (pure DMSO) to 78.36 (pure water).[35] The conductivity of two FLN ionomer solutions have different dependence with solution composition (**Fig. 2b**). The exponential decay curve fitting of conductivity and dielectric constant data of water-DMSO mixture solvents shows that the FLN-100 has much higher dependence (a = 0.523, b =208.4) then FLN-55 (a = 0.067, b = 88.25), suggesting that the number of mobile charge carriers for FLN-100 increases more significantly as the cationic functional group is solvated in the medium. As a result, the conductivity of FLN-100 is higher than that of FLN-55 at > 30% water. At the lower water content, the hydroxide conductivity of FLN-100 was lower than that of FLN-55. The hydroxide conductivity of FLN-100 at 100% water was estimated to 37 mS cm^{-1}, which is about 70% higher than that of FLN-55 (22 mS cm^{-1}). Considering that FLN-100 is extremely hygroscopic than FLN-55 (water uptake for FLN-100: > 2,000 wt.% vs. 180 wt.% for FLN-55),[36] FLN-100 may retain a substantial amount of water to provide enough conductivity for the electrochemical reactions and low cell resistance under low RH conditions.

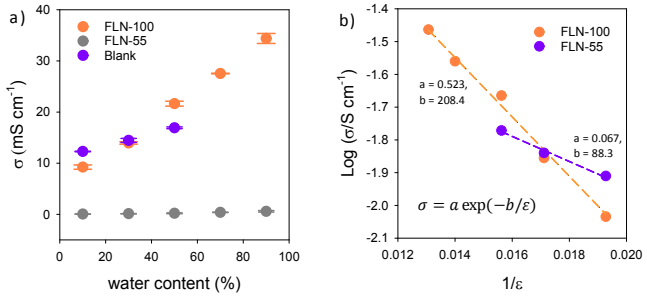

Fig. 2 (a) Hydroxide conductivity (σ) of FLNs in DMSO/water mixture as a function of water content at 80 °C, (b) Conductivity as a function of the reverse of dielectric constant of water-DMSO mixture.

AEMFC performance of symmetric electrode ionomer

We investigated the optimum RH conditions of two MEAs with symmetric electrode ionomer (the same ionomer for both anode and cathode) at the anode and cathode. Symmetric cells are the standard method of cell evaluation and serve as control MEAs to investigate their optimum RH conditions. MEA1 and MEA2 used FLN-55 and FLN-100, respectively, for both anode and cathode ionomeric binders. To understand the hydration state of the anode and cathode, we recorded the transient hysteresis behaviour by polarization curves[37] during the forward and backward sweeps. We applied symmetric

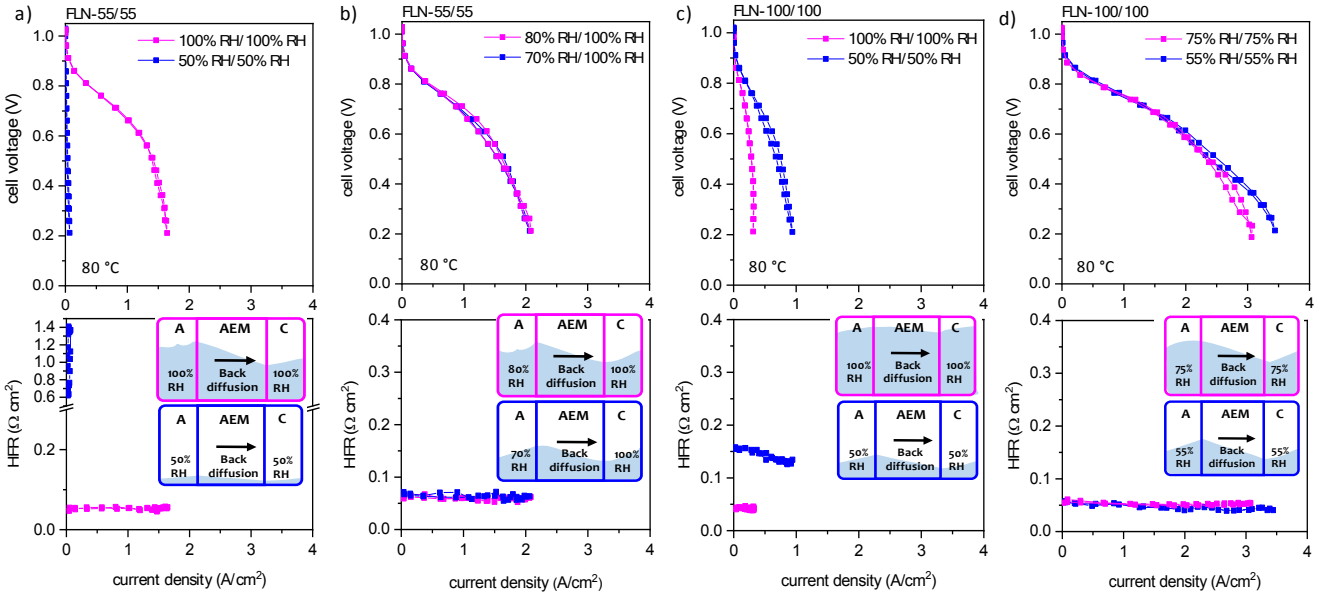

Fig. 3 H_2/O_2 AEMFC performance of using symmetric electrode ionomer (a) MEA1 either at 100% RH or 50% RH on both anode and cathode, (b) MEA1 at optimum humidification, (c) MEA2 either at 100% RH or 50% RH on both anode and cathode, (d) MEA2 at optimum humidification. The inset figures schematically explain the hydration of the MEA component at high current density.

RHs to the anode and cathode (100–50%) and asymmetric RHs in which the RH of one electrode was fixed to 100% and the RH of the other electrode changed from 90% to 50%.

Fig. 3a shows the polarization curves of MEA1 in which FLN-55 ionomer was used for both the anode and cathode under fully humidified (100% RH) and partially humidified (50% RH) conditions. High performance was obtained at 100 % RH with a little hysteresis. The slightly higher current density was obtained during the forward scan (increasing current density direction), suggesting minor flooding at the water generating (anode) electrode. At 50 % RH, the MEA showed poor performance. Extremely elevated high-frequency resistance (HFR, 0.5–1.5 Ω cm^{-2}) indicates that the MEA was substantially dehydrated. We further evaluated the MEA performance under different humidification to find the optimum RH conditions. The highest performance of MEA1 was obtained at 80% RH anode/100% RH cathode and 70% RH anode/100% RH cathode (**Fig. 3b**). The performance of MEA1 at 80% and 70% RH anode is almost identical, which indicated that the performance sensitivity of the anode RH with FLN-55-bonded MEA is lower than to polyolefinic ionomer-bonded MEA.[23] The optimum RHs for MEA1 was consistent with the expectation that the performance of MEA1 at 100% RH anode (**Fig. 3a**) will result in mass transport losses at high current densities, ca. > 1 A cm^{-2}. The performance improvement from 100% RH conditions to the lower anode humidification is notable (1.6 to 2.1 A cm^{-2} at 0.2 V). The HFR of MEA1 with an anode of 70–80% RH was only slightly higher (~0.01 Ω cm^2) than that of MEA1 at 100% RH and was stable with the current density. These results indicate that the impact of anode flooding is more detrimental than AEM dehydration with these anode RH changes. The little hysteresis and stable HFR with current density suggest that the AEM was still well hydrated at high current density by back diffusion of water (inset figure).

MEA2, in which FLN-100 was used for both anode and cathode ionomeric binder, showed superior performance at 50% RH compared to 100% RH (**Fig. 3c**). At 100% RH, the fuel cell performance was poor due to the significant flooding at the anode, as noted by the cell performance suppression at the high current density region. At 50% RH, flooding at the anode no longer occurs, but MEA2 was partially dehydrated (HFR = 0.15 Ω cm^{-2}). The superior MEA2 performance at 50% RH to the MEA1 performance under the same condition confirmed that FLN-100 ionomer could hold more water in the electrodes, better suited to low RH operation. **Fig. 3d** shows the AEMFC performance of MEA2 at optimum humidification. The highest performance of MEA2 was obtained at symmetric humidification of 55% to 75% RH. Note that only a 5% RH increase prevented MEA dehydration and results in a significant performance improvement from the 50% RH operation shown in **Fig. 3c**. This result suggests that under 50% RH, issues of AEM dehydration and also reactant water deficit may cause the poor performance, as minute increases of humidity will not result in large conductivity changes. Also, the performance obtained with the FLN-100 ionomer at 55% RH was higher than the best performance of the FLN-55 ionomer-bonded MEA under nearly fully humidified conditions. At 75% RH, the performance of MEA2 was slightly lower at the current density > 2.5 A cm^{-2} due to slight anode flooding. The HFR of MEA2 at 75% RH was 0.05 Ω cm^{-2}, similar to the flooded anode shown in **Figure 3c**. The optimum RH conditions for MEA2 were achieved with the same RH at the anode and cathode by back diffusion of water from the anode to cathode (inset figure).

AEMFC performance of asymmetric electrode ionomer

Next, we investigated the AEMFC performance of asymmetric electrode ionomer at the anode and cathode. We fabricated two MEAs: MEA3 used FLN-55 in the anode binder and FLN-100 in the cathode binder and MEA4 used the opposite combination to MEA3,

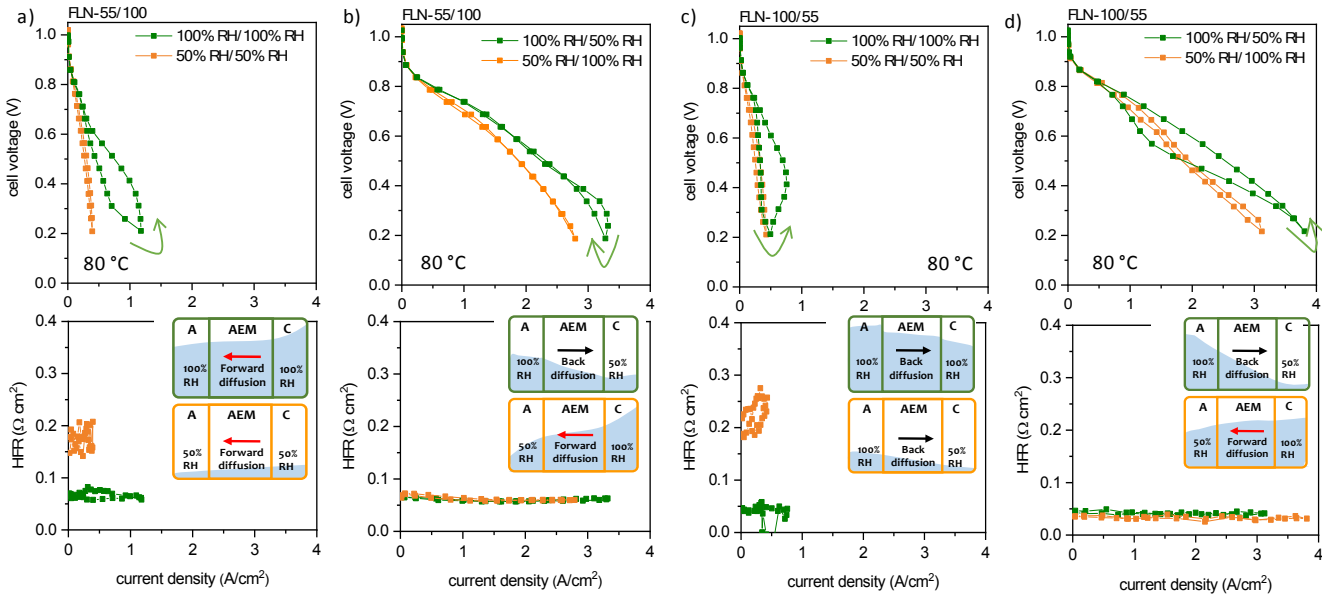

Fig. 4 H_2/O_2 AEMFC performance of using asymmetric electrode ionomer (a) MEA3 either at 100% RH or 50% RH on both anode and cathode, (b) MEA3 at asymmetric humidification, (c) MEA4 either at 100% RH or 50% RH on both anode and cathode, (d) MEA4 at asymmetric humidification. The inset figures schematically explain the hydration of the MEA component at high current density.

i.e., FLN-100 for the anode ionomeric binder and FLN-55 for the cathode ionomeric binder. The performance of MEA3 (FLN-55/100) at 100% RH was substantially lower than the symmetric MEA1 (FLN-55/55) at 100% RH (**Fig. 4a**). The presence of the more hygroscopic FLN-100 ionomer in MEA3 exacerbated flooding, which leads to significant hysteresis during the backward scan. Because the water content of the cathode in MEA3 is higher than in the anode, water diffusion likely occurs from cathode to anode (forward diffusion) even at high current density, although an accurate net water flux measurement is required to confirm this. Considering that the flooding of the FLN-55 anode at 100% RH is moderate, since the maximum current is limited < 1.5 A cm^{-2}, the flooding likely occurs at the cathode instead of the anode. At 50% RH, MEA3 suffered from drying out, reflected by the increased HFR, due to the less hygroscopic FLN-55 ionomer. The dry out in MEA3 was less severe than for MEA1, yet more severe than for MEA2. We tested the MEA3 performance under asymmetric humidification. **Fig. 4b** shows the MEA3 performance under two asymmetric humidification conditions, i.e. 100 RH% (anode)/50% RH (cathode) and 50 RH% (anode)/100% RH (cathode). Under these asymmetric humidification conditions, MEA3 exhibited greater performance compared to the MEA3 under symmetric humidification. MEA3 under 100%/50% RH (anode/cathode) showed slightly higher performance than that under 50%/100% RH (anode/cathode). It is important to note that the performance of MEA3 under 50%/100% RH was obtained via forward diffusion of water (cathode to anode) instead of back diffusion that most high-performing AEMFCs require (inset figure).

The performance of MEA4 (FLN-100/55) under symmetric RH conditions was poor, similar to the performance of MEA3 (**Fig. 4c**). Because we used the hygroscopic FLN-100 ionomer at the anode, the water diffusion is in the backward direction, the opposite direction to the MEA3. Under asymmetric humidification, i.e., 100 RH% (anode)/50% RH (cathode) and 50 RH% (anode)/100% RH (cathode), the AEMFC performance of MEA4 improved significantly, and two asymmetric humidification conditions afforded a similar performance. These results indicate that high AEMFC performance can be achieved by forward diffusion of water when a highly asymmetric MEA structure is used under proper humidification. The peak power density of symmetric MEA2 and asymmetric MEA3 and MEA4 under their optimum humidification are comparable, ranging from 950–1260 mW cm^{-2}. Since these MEAs exhibit excellent performance under low RH conditions compared to MEA1 under nearly full-hydrated conditions, we examined their AEMFC durability under reduced RH conditions to select the best MEA and operating conditions.

AEMFC durability

A short-term durability test up to 100 h at a constant current density of 0.6 A cm^{-2} for all MEAs was examined under specific RH conditions to down select the best MEA and operating conditions. The symmetric MEA1 (FLN-55/55) exhibited a constant performance loss with increasing cell resistance over 100 h under fully humidified conditions (**Fig. 5a**). MEA2 (FLN-100/100) operated under reduced humidity, 55% RH anode and cathode, exhibited the most substantial performance loss, although the initial cell voltage of MEA2 was higher than that of MEA1 (**Fig. 5b**). The cell stopped working within 20 h of operation. These results suggest that continuous cell operation under low RH conditions may shorten the lifetime of the MEA. To understand which electrode is more sensitive to low RH operation, we evaluated the durability of MEA3 and MEA4 under asymmetric RH conditions. For MEA3 (FLN-55/100), the durability was much lower under low anode RH (50% anode/100% cathode) than that under higher anode RH (100% anode/50% cathode) (**Figs. 5c** and **d**). Surprisingly, the durability of MEA3 under

high anode and low cathode RH conditions was even better than that of MEA1 under fully hydrated conditions. A similar trend was observed with MEA4 (FLN-100/55) (**Figs. 5e,** and **5f**); the durability of MEA4 under low anode humidification and high cathode humidification was much shorter than the same MEA under high anode humidification and low cathode humidification.

The enhanced durability of the MEAs under low cathode RH

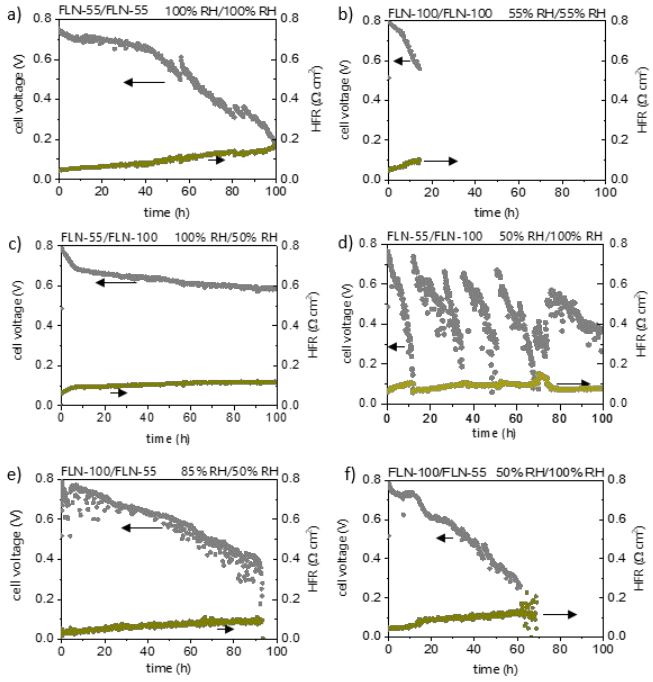

Fig. 5 100 h short-term durability test (a) MEA1 at 100% RH anode and 100% RH cathode, (b) MEA2 at 55% RH anode and 55% RH cathode, (c) MEA3 at 100% RH anode and 50% RH cathode, (d) MEA3 at 50% RH anode and 100% RH cathode, (e) MEA4 at 85% RH anode and 50% RH cathode, (f) MEA4 at 50% RH anode and 100% RH cathode. The short-term test was performed at a constant current density of 0.6 A cm^{-2} under 1400/300 sccm H_2/O_2 at 147.5 kPa backpressure and 80°C.

conditions is counterintuitive considering the cathode ionomer degradation is thought to be accelerated under reduced RH conditions.[19-21] However, it may be understandable since ionomer degradation is expected only at very low hydration numbers (λ), ca. ≤ 4.[19] To understand the possible degradation mechanism of the MEA under low anode RH and high cathode RH, we replenished MEA3 under 50%/100% RH (anode/cathode) that showed low durability by flowing 1.0 M NaOH solution.[36] **Fig. 5d** shows that the most cell performance of MEA3 was recovered after the replenishing process, although the total lifetime of the MEA3 under 50% anode RH and 100% cathode RH was much shorter (< 100 h) than that of the MEA3 under 100% anode RH and 50% cathode RH. This experiment suggests the performance degradation of the MEA3 in **Fig. 5d** likely occurred with electrochemical oxidation of carbon (Eq. 1) at the cathode, which impacts both recoverable and unrecoverable performance degradation.

$$C + 2H_2O \rightarrow CO_2 + 4H^+ + 4e^- \quad (1)$$

Since the electrochemical oxidation of carbon requires water as a reactant, it can occur faster with higher water levels at the electrode.[38] The generated CO_2 transformed to CO_3^{2-}, which is then transported to the anode.[39] When the hydration level of the anode is low, the CO_3^{2-} accumulates more quickly at the anode and the overall AEMFC performance decreases. The replenishing process with NaOH solution helps to recover the performance by removing the accumulated carbonated species. The electrochemical oxidation of carbon also results in a shorter lifetime because the phenyl group in the quaternized ionomer was converted to the acidic phenolic compound.[34] These short-term test results suggest that while some MEAs showed good beginning of life performance under low anode and high cathode RH conditions, those conditions are not advantageous for long-term MEA operation. This result is also consistent with the fact that a majority of durable AEMFC literature operate at high current conditions, e.g. 0.6 A cm^{-2}, in which a significant amount of water is consumed by the ORR and the cathode potential is low.[1, 40, 41] Therefore, we concluded that the best MEA is the asymmetric MEA3 (FLN-55/100) operated under high anode RH and low cathode RH conditions.

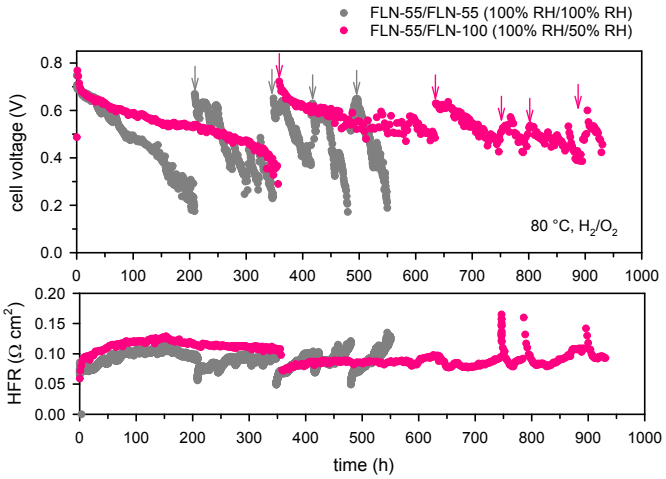

Fig. 6 The cell voltage and HFR change of MEA1 (FLN-55/FLN-55) and MEA3 (FLN-55/FLN-100) during the H_2/O_2 operation at 0.6 A cm^{-2} over time. Humidifiction: MEA1 (anode 100% RH/cathode 100% RH) and MEA3 (anode 100% RH/cathode 50% RH). The arrows denote the cell replenishment process with NaOH solution during the life test.

Next, we investigated the long-term stability of MEA3 under 100% RH anode and 50% RH cathode conditions at a constant current of 0.6 A cm^{-2}. In the long-term stability testing, we replenished the cell when the cell voltage loss was significant, < 0.2 V. **Fig. 6** compares the voltage and HFR change of MEA3 with a control sample (MEA1) under fully humidified conditions, which we have reported in a previous paper.[34] The voltage decay rate of MEA3 for the first 200 h was 1.1 mV h^{-1}; only 42% of that of MEA1 (2.6 mV h^{-1}), despite the similar HFR changes in both MEAs. Most of the voltage loss was recovered by replenishment with NaOH solution, indicating that carbonated species of the anode was removed. We have identified the source of carbonation from CO_2 in the condensed water used for humidification.[34] Another more likely source is the oxidation of the carbon-based cell components on the cathode. The lifetime of MEA3

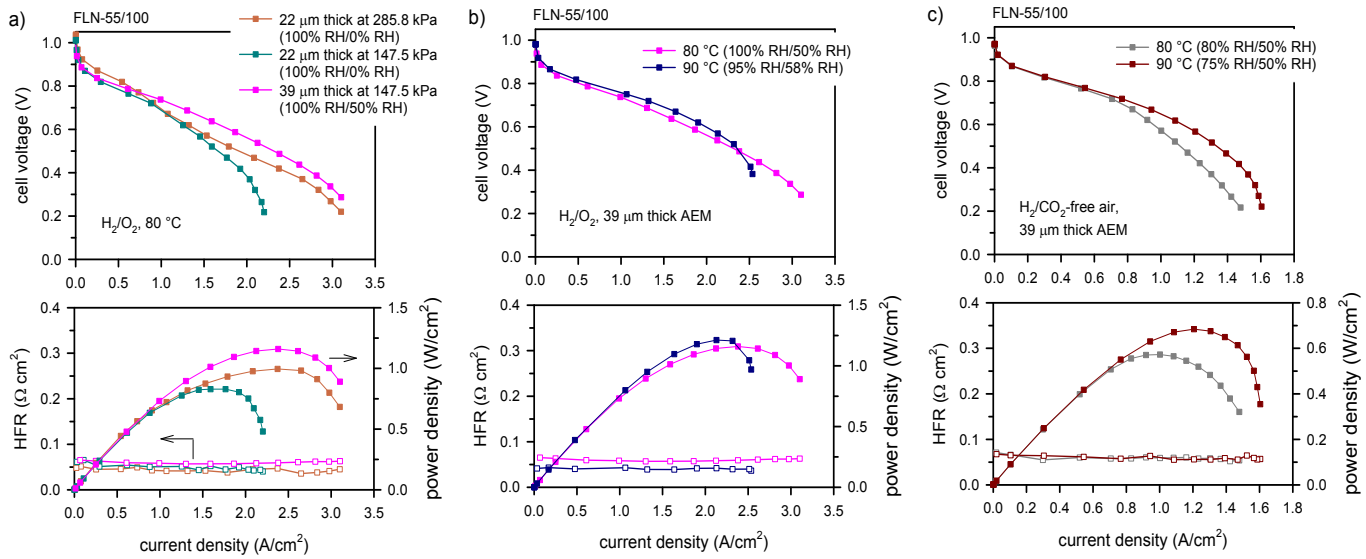

Fig. 7 (a) Effect of AEM thickness. The H_2/O_2 fuel cell performance of MEA3 using 22 μm- and 39 μm-thick AEMs. (b) Effect of operating temperatures; H_2/O_2 fuel cell performance of MEA3 using a 39 μm-thick AEM at 80 and 90 °C under optimized RH conditions. (c) H_2/CO_2–free air AEMFC performance of MEA3 using a 39 μm-thick AEM at 80 and 90 °C under optimized RH conditions.

could be extended to 933 h after five replenishment processes, which was 1.7 times longer than the lifetime of MEA1 (550 h) under reduced cathode RH conditions. The experiment was ended at 933 h after a test station control error caused the cell to fail. The longer lifetime of MEA3 indicates that the electrochemical oxidation of FLN-100 at the cathode under 50% RH conditions was less than that of FLN-55 under 100% RH conditions.

Impacts of AEM thickness, operating temperature and CO_2-free air

Thinner AEMs can facilitate water transport of back diffusion-controlled MEAs by lowering the transport barrier for cross-membrane water flow.[14] Therefore, further reduction of cathode humidification could be obtained with a thinner AEM without sacrificing performance. We investigated the impact of AEM thickness (*t*) on AEMFC performance using 22 μm-thick AEM. **Fig. 7a** compares the AEMFC performance of MEA3 using the 22 μm-thick and the 39 μm-thick AEMs. Note that a comparable performance at the current density of < 1.5 A cm^{-2} was obtained with the MEA using 22 μm-thick AEM under 0% RH cathode conditions in which all of the required water for AEM hydration and ORR was supplied from the anode. At higher current densities, ca. > 1.5 A cm^{-2}, MEA3 using the thinner AEM exhibited a slightly lower performance, probably due to the deficit of reactant water at the cathode. Increasing the back pressure to 285 kPa helped to push more water to the cathode, thus improving performance. Note that all of these performance changes were obtained by manipulating the water management; and therefore, cell resistance plays a negligible role.

The operating temperature impact of water transport on back diffusion-controlled MEAs is complex, as several properties of the MEA components change with increasing temperature and influence each other. First, higher temperature operation increases the reaction kinetics of the HOR and ORR catalysts, resulting in more water generation at the anode and more water consumption at the cathode. Second, the water permeability increases and facilitates the back diffusion of water. Third, water evaporation increases both at the anode and cathode, which makes it difficult for full AEM hydration. Fourth, the hydroxide conductivity of polymer electrolytes increases. We optimized the RH conditions of MEA3 at the operating temperature of 90 °C and compared the performance at 80 °C. **Fig. 7b** compares the optimized performance of MEA3 at 90 °C with that at 80 °C. It was noted that the optimized performance at 90 °C was obtained with slightly higher cathode humidification, suggesting that cathode dehydration could not be fully compensated by faster back diffusion. The kinetic performance (cell voltage > 0.75 V) of MEA3 at 90 °C was higher, yet the cell performance at the high current density region was slightly lower. Hydration of AEMs with slightly higher cathode RH seems to be less problematic, as we obtained lower HFR at 90 °C. These results suggest that the higher temperature operation causes a water deficit at the cathode, which cannot be compensated fully by faster water back diffusion. In general, lowering RH for AEMFC MEAs is more challenging with higher operating temperature.

We investigated the impact of CO_2-free air *vs* O_2 on AEMFC performance. **Fig. 7c** shows the optimized H_2/ CO_2-free air AEMFC performance at the operating temperature of 80 and 90 °C. It was noted that the optimized RH conditions for the H_2/CO_2-free air AEMFC were similar to H_2/O_2 AEMFC, i.e., 80% anode RH/50% cathode RH. At 80 °C, the H_2/CO_2-free air peak power density is 50% of the H_2/O_2 peak power density. At 90 °C, however, the H_2/CO_2-free air peak power density was 685 mW cm^{-2}, 57% of the H_2/O_2 peak power density (1,210 mW cm^{-2}), probably because the H_2/O_2 performance at 90 °C was limited by cathode dehydration. We compared the AEMFC performance to those of state-of-the-art AEMFCs in terms of rated power density (RPD) in which the heat rejection requirement for automotive fuel cells is met.[15] The H_2/CO_2-free air RPD obtained with MEA3 at 80 and 90 °C was 380 (0.76 V) and 540 mW cm^{-2} (0.69 V), respectively. The rated power density we

obtained under the reduced RH conditions were comparable to those of the state-of-the-art AEMCs under nearly water-saturated conditions (**Table 1**). [3, 6, 7, 35, 42, 43]

Table 1 H_2/CO_2-free air RPD comparison with state-of-the-art AEMFCs.

MEA (AEM/ionomer)	*t* (μm)	T (°C) Cell/ An/Ca	RPD (mW cm^{-2})	Ref.
HTMA-DAPP/FLN-55 (A), FLN-100 (Ca)	39	90/82/73	540	This work
HTMA-DAPP/FLN-55 (A), FLN-100 (Ca)	39	80/75/64	380	This work
Poly(norbornene)/ETFE-*g*-poly(VBTMAC)[a]	10	80/70/78	760	41
PAP-TP-85 AEM/PAP-BP-100[b]	25	95/94/95	635	3
LDPE AEM/ETFE-*g*-poly(VBTMAC)[c]	25	80/78/78	486	36, 43
m-TPN/FLN[d]	30	80/80/80	393	36
Reinforced composite/proprietary[e]	25	80/?/?	365	6

[a]ETFE-*g*-poly(VBTMAC): poly(ethylene-*co*-tetrafluoroethylene)-*g*-poly(vinylbenzylrimethylammonium chloride), [b]PAP-TP: poly(aryl peperidinium)-terphenyl, used low Pt loading anode and Ag-based cathode [c]LDPE: low density polyethylene, [d]*m*-TPN: *meta*-poly(terphenylene), FLN: poly(fluorene); [e]used low loading Pt anode.

Conclusions

Operating AEMFCs under hot and reduced RH conditions is desirable for automotive fuel cell applications. In this paper, we have demonstrated high performance and durable AEMFCs under reduced RH conditions for the first time through asymmetric electrode ionomer. Utilizing highly quaternized hygroscopic ionomer (FLN-100, IEC = 3.5 meq. g^{-1}) at the cathode maintains the required water level for the cathode reaction without fully hydrated conditions. The performance advantage of Ionomers with high ammonium concentration has been recently proposed in the AEM electrolyzer,[44] and this research suggests the benefit for AEMFCs low RH operation for the first time. This paper also shows that high AEMFC performance (~1.0 W cm^{-2} peak power density) could be obtained via non-conventional forward diffusion of water using an asymmetric MEA design. However, the performance degradation of the MEAs with the forward water diffusion is high due to electrochemical oxidation of the cathode materials under the required high cathode RH conditions. The durability of an asymmetric MEA (FLN-55/FLN100) with water back diffusion is superior to the previous symmetric MEA operating under nearly fully hydrated conditions. We demonstrated > 930 h lifetime for the MEA at a constant current density of 0.6 A cm^{-2}, 80 °C, H_2/O_2 and under reduced cathode RH conditions (50%). We also demonstrated that further reduction of cathode RH to 0% is possible without significant performance loss by decreasing AEM thickness to 22 μm. Increasing the temperature to 90 °C made water management difficult, thus minimal performance improvement was observed. However, switching from H_2/O_2 to H_2/CO_2-free air helped water management as less current density was generated. We achieved the rated power density of 540 mW cm^{-2} at 90 °C under 75% anode RH and 50% cathode RH conditions, which is comparable to those of state-of-the-art symmetric AEMFCs under nearly fully humidified conditions. This research provides insights into how AEMFCs can operate under reduced RH conditions, which has been considered one of the most challenging tasks of commercially viable AEMFCs, but a must for the automotive fuel cell application.

Experimental

Preparaion of FLN ionomer dispersion

Quaternized poly(fluorene)s (FLNs) were synthesized via one-pot, acid-catalysed Freidel-Crafts polycondensations of 1,1,1-trifluoroacetone and fluorene monomers and subsequent amination with trimethylamine as described in the previous paper.[35] FLNs in bromide ion form were converted to hydroxide form by soaking in a 1 M NaOH solution for 48 h and thoroughly washed with degassed deionized water until pH became neutral. The FLN ionomers in hydroxide form are soluble in methanol, dimethylsulfoxide, and *N*-dimethylformamide at room temperature but insoluble in water, acetone, and tetrahydrofuran. Therefore, the catalyst dispersions were prepared from the OH^- form of FLN ionomer dispersions in an alcoholic solvent mixture.

Preparation of HTMA-DAPP AEM

Hexyltrimethylammonium functionalized poly(phenylene) (HTMA-DAPP) was synthesized by an irreversible Diels-Alder reaction as described in the previous paper.[45, 46] First, brominated alkyl ketone functionalized Diels-Alder poly(phenylene) was synthesized by reacting DAPP with 6-bromohexanoyl chloride in the presence of aluminum chloride. The ketone group of the polymer was reduced to the methyllene group by reduction with trifluoroacetic acid and triethylsilane. The brominated polymer was cast onto a glass plate from chloroform. After drying, the membrane was aminated by immersion in trimethylamine solution (45% w/w in water) for 48 h. The resulting membrane was then immersed in 0.5 M HBr for 2 h to convert the membrane in a brominated form. The brominated membrane was converted hydroxide form by immersing in 0.5 M NaOH at 80 °C. The thickness of the membrane was either 22 or 39 μm. The water uptake of hydroxide form of HTMA-DAPP was 58% at 30°C.[18] Hydroxide conductivity of the membrane is 120 mS cm^{-1} at 80°C.[18]

Hydroxide conductivity measurement

Hydroxide conductivity measurements of ionomer solutions were carried out using AC impedance spectroscopy on a Solartron 1260 gain phase analyser in the 1 MHz to 1 Hz frequency range. Ionomer solutions of FLN-100 and FLN-55 in the hydroxide form were prepared by first dissolving 100 mg of ionomer in the appropriate quantity of dry DMSO, (10, 30, 50, 70, 90 wt% assuming a 2.00 g final mass). Once dissolved, the appropriate quantity of 18 MΩ H_2O was added to achieve the desired water content (10, 30, 50, 70, 90 wt% H_2O). Prior to testing, the solutions were allowed to stand at 60 °C until full dissolution was achieved. Each solution was loaded into a liquid measurement cell and then allowed to equilibrate to 80 °C for 1 h prior to executing the measurement. Conductivity (σ, S cm^{-1}) was calculated from the equation below:

$$\sigma = \frac{L}{R \times A} \quad (2)$$

where L (cm) is the distance between the electrode faces, R (Ω) is the resistance at the intercept bertween the Re (Z) axis and the high frequency complex impedance plane, and A (cm^2) is the area of the electrode face.

Preparation of MEAs

Gas diffusion electrodes (GDEs) were prepared using catalyst inks, of Pt/C for cathodes (60 wt% Pt, on HISPEC® 9100, Alfa Aesar) and PtRu/C (50 wt% Pt, 25 wt% Ru, on HISPEC® 12100, Alfa Aesar) for anodes, and hand painted onto 5 cm^2 sections cut from SGL 29BC (Sigracet®) gas diffusion layer material. Catalyst inks were prepared by weighing 20.0 mg catalyst, 69.2 mg of 5 wt% ionomer solution, and 2.00 g of 80/20 wt% IPA/H_2O solution into a vial and sonicated for 1 h in a sonication bath prior to painting. Each vial of catalyst ink was used to paint two 5 cm^2 electrodes until a final loading of 0.6 mg_{Pt} cm^{-2} for cathodes and 0.75 mg_{PtRu} cm^{-2} for anodes were achieved. GDEs were allowed to dry at room temperature for 18 h. Before assembly into MEAs, GDEs and membranes were allowed to soak in 1 M NaOH for 2 h.

Fuel cell performance test and durability evaluation

Immediately after the 2 h, 1 M NaOH solution soak and subsequent rinsing with deionized water, the MEA was assembled into a Fuel Cell Technologies test cell and connected to the Fuel Cell Technologies test station for break-in. The cell was brought up to 65°C, and gas flow was initiated with H_2/O_2 at 1400/700 sccm and 147.5 kPa and 100% RH. Cell voltage was held at a constant 0.5 V. Break-in started once cell temperature reached 80°C. During break-in the cell was held at 0.5 V in constant voltage mode for at least 2 h. Cells that were run at reduced RH were held at 100% RH for the first hour, and then the RH was lowered to 50%. Cell voltage remained constant during this process. After break-in the cell was allowed to cool before alkaline treatement with 1 M NaOH.

The following day, prior to testing, the cell was once again flushed with 1 M NaOH and subsequent rinsing with deionized water, attached to the test station, and brought up to temperature as before. Cell votltage was set to 0.5 V, 100% RH, 1400/700 sccm H_2/O_2, and 147.5 KPa backpressure. Once constant current was observed, usually after 3 h, polarization curves were taken. For cells operating at low RH, after the first hour under constant voltage, the RH setpoint was changed to 50% RH and allowed to run until both RH and current had stabilized. At that point polarization curves were taken. For cells operated at 0% RH on the cathode, the cell began under 100% RH. Cathode RH was reduced to 50% RH and allowed to run until current stabilized, then the humidity bottle was bypassed to achieve 0% RH. Polarization curves were taken after the current stabilized. For cells using elevated temperature and CO_2-free air break-in took place as described above in H_2/O_2 at 80°C. The cells were then brought up to temperature. Before polarization curves were taken, cathode-reactant gas was changed from O_2 to CO_2-free air, the current was allowed to stabilize, and RH was optimized. Reactant gas flow rates remained the same, 1400/700 sccm H_2/CO_2-free air, during testing.

Once initial performance was established, durability tests could begin. For these tests the fuel cell test station operation was changed from 0.5 V and constant voltage mode to 0.6 A cm^{-2} constant current mode. Cathode flow rate was decreased from 700 sccm to 300 sccm. During durability tests, when cell voltage decayed to 0.2 V the test was suspended and the cell was treated with NaOH.[34] Upon resuming the test, the cell was broken in as before and the durability test restarted once constant current was observed.

Conflicts of interest

There are no conflicts to declare.

Acknowledgements

This work was supported by the US Department of Energy, Energy Efficiency and Renewable Energy, Fuel Cell Technologies Office (FCTO). Los Alamos National Laboratory is operated by Triad National Security, LLC under U. S. Department of Energy Contract Number 89233218CNA000001. CB also thanks ARPA-E (IONICS DE-AR0000769) for financial support.

Notes and references

1. G. Huang, M. Mandal, X. Peng, A. C. Yang-Neyerlin, B. S. Pivovar, W. E. Mustain and P. A. Kohl, *J Electrochem Soc*, 2019, **166**, F637-F644.
2. T. J. Omasta, A. M. Park, J. M. Lamanna, Y. Zhang, X. Peng, L. Wang, D. L. Jacobson, J. R. Varcoe, D. S. Hussey, B. Pivovar and W. E. Mustain, *Energ Environ Sci*, 2018, **11**, 551-558.
3. J. H. Wang, Y. Zhao, B. P. Setzler, S. Rojas-Carbonell, C. Ben Yehuda, A. Amel, M. Page, L. Wang, K. Hu, L. Shi, S. Gottesfeld, B. J. Xu and Y. S. Yan, *Nature Energy*, 2019, **4**, 392-398.
4. H. G. Peng, Q. H. Li, M. X. Hu, L. Xiao, J. T. Lu and L. Zhuang, *J Power Sources*, 2018, **390**, 165-167.
5. E. J. Park, S. Maurya, A. S. Lee, D. P. Leonard, D. Li, J. Y. Jeon, C. Bae and Y. S. Kim, *J Mater Chem A*, 2019, **43**, 25040-25046.
6. S. Noh, J. Y. Jeon, S. Adhikari, Y. S. Kim and C. Bae, *Accounts Chem Res*, 2019, **52**, 2745-2755.
7. L. Q. Wang, J. J. Brink, Y. Liu, A. M. Herring, J. Ponce-Gonzalez, D. K. Whelligan and J. R. Varcoe, *Energ Environ Sci*, 2017, **10**, 2154-2167.
8. Y. Wang, Y. Yang, S. F. Jia, X. M. Wang, K. J. Lyu, Y. Q. Peng, H. Zheng, X. Wei, H. Ren, L. Xiao, J. B. Wang, D. A. Muller, H. D. Abruna, B. O. E. Hwang, J. T. Lu and L. Zhuang, *Nat Commun*, 2019, **10**.
9. X. Peng, T. J. Omasta, E. Magliocca, L. Q. Wang, J. R. Varcoe and W. E. Mustain, *Angew Chem Int Edit*, 2019, **58**, 1046-1051.
10. R. Wang, D. Li, S. Maurya, Y. S. Kim, Y. Wu, Y. Liu, D. Strmcnik, N. M. Markovic and V. R. Stamenkovic, *Nanoscale Horizons*, 2019, DOI: 10.1039/C9NH00533A, in print.
11. T. J. Omasta, Y. F. Zhang, A. M. Park, X. Peng, B. Pivovar, J. R. Varcoe and W. E. Mustain, *J Electrochem Soc*, 2018, **165**, F710-F717.
12. A. Roy, M. R. Talarposhti, S. J. Normile, I. V. Zenyuk, V. De Andrade, K. Artyushkova, A. Serov and P. Atanassov, *Sustain Energ Fuels*, 2018, **2**, 2268-2275.
13. F. L. Yang, X. Bao, P. Li, X. W. Wang, G. Z. Cheng, S. L. Chen and W. Luo, *Angew Chem Int Edit*, 2019, **58**, 14179-14183.
14. S. Gottesfeld, D. R. Dekel, M. Page, C. Bae, Y. S. Yan, P. Zelenay and Y. S. Kim, *J Power Sources*, 2018, **375**, 170-184.

15. R. K. Ahluwalia, X. Wang and A. J. Steinbach, *J Power Sources*, 2016, **309**, 178-191.
16. A. Kongkanand and M. F. Mathias, *J Phys Chem Lett*, 2016, **7**, 1127-1137.
17. M. R. Sturgeon, C. S. Macomber, C. Engtrakul, H. Long and B. S. Pivovar, *J Electrochem Soc*, 2015, **162**, F366-F372.
18. E. J. Park, S. Maurya, M. R. Hibbs, C. H. Fujimoto, K. D. Kreuer and Y. S. Kim, *Macromolecules*, 2019, **52**, 5419-5428.
19. D. R. Dekel, M. Arnar, S. Willdorf, M. Kosa, S. Dhara and C. E. Diesendruck, *Chem Mater*, 2017, **29**, 4425-4431.
20. D. R. Dekel, S. Willdorf, U. Ash, M. Amar, S. Pusara, S. Dhara, S. Srebnik and C. E. Diesendruck, *J Power Sources*, 2018, **375**, 351-360.
21. K. D. Kreuer and P. Jannasch, *J Power Sources*, 2018, **375**, 361-366.
22. H. Deng, D. W. Wang, X. Xie, Y. B. Zhou, Y. Yin, Q. Du and K. Jiao, *Renew Energy*, 2016, **91**, 166-177.
23. T. J. Omasta, L. Wang, X. Peng, C. A. Lewis, J. R. Varcoe and W. E. Mustain, *J Power Sources*, 2018, **375**, 205-213.
24. M. G. Marino, J. P. Melchior, A. Wohlfarth and K. D. Kreuer, *J Membrane Sci*, 2014, **464**, 61-71.
25. S. Huo, J. X. Zhou, T. Y. Wang, R. Chen and K. Jiao, *J Power Sources*, 2018, **382**, 1-12.
26. M. Mandal, G. Huang, N. Ul Hassan, X. Peng, T. L. Gu, A. H. Brooks-Starks, B. Bahar, W. E. Mustain and P. A. Kohl, *J Electrochem Soc*, 2019, **167**.
27. S. Jang, M. Her, S. Kim, J. H. Jang, J. E. Chae, J. Choi, M. Choi, S. M. Kim, H. J. Kim, Y. H. Cho, Y. E. Sung and S. J. Yoo, *Acs Appl Mater Inter*, 2019, **11**, 34805-34811.
28. R. B. Kaspar, M. P. Letterio, J. A. Wittkopf, K. Gong, S. Gu and Y. S. Yan, *J Electrochem Soc*, 2015, **162**, F483-F488.
29. T. Reshetenko, M. Odgaard, D. Schlueter and A. Serov, *J Power Sources*, 2018, **375**, 185-190.
30. E. J. Park and Y. S. Kim, *J Mater Chem A*, 2018, 6, 15456-15477.
31. C. Fujimoto, D. S. Kim, M. Hibbs, D. Wrobleski and Y. S. Kim, *J Memb Sci*, 2012, **423**, 438-449.
32. I. Matanovic, S. Maurya, E. J. Park, J. Y. Jeon, C. Bae and Y. S. Kim, *Chem Mater*, 2019, **31**, 4195-4204.
33. I. Matanovic, H. T. Chung and Y. S. Kim, *J Phys Chem Lett*, 2017, **8**, 4918-4924.
34. S. Maurya, A. S. Lee, D. G. Li, E. J. Park, D. P. Leonard, S. Noh, C. Bae and Y. S. Kim, *J Power Sources*, 2019, **436**.
35. A. M. Affoune, A. Yamada M. Umeda, *J Power Sources*, 2005, **148**, 9-17.
36. S. Maurya, S. Noh, I. Matanovic, E. J. Park, C. N. Villarrubia, U. Martinez, J. Han, C. Bae and Y. S. Kim, *Energ Environ Sci*, 2018, **11**, 3283-3291.
37. J. Hou, *Int J Hydrogen Energ*, 2011, **36**, 7199-7206.
38. B. Pivovar and Y. S. Kim, *2019 Anion Exchange Membrane Workshop Summary Report*, Dallas, Texas, 2019.
39. B. P. Setzler and Y. Yan, *The Electrochemical Society Meeting Abstracts*, 2017, **2017**, 1654.
40. Y. W. Zheng, T. J. Omasta, X. Peng, L. Q. Wang, J. R. Varcoe, B. S. Pivovar and W. E. Mustain, *Energ Enveron Sci*, 2019, **12**, 2806-2819.
41. B. Pivovar, *2019 Annual Merit Review Proceedings* 2019, https://www.hydrogen.energy.gov/pdfs/review19/fc178_pivovar_2019_o.pdf.
42. M. Mandal, G. Huang, N. U. Hassan, X. Peng, T. Gu, A. H. Brooks-Starks, B. Bahar, W. E. Mustain and P. A. Kohl, *J Electrochem Soc*, 2020, **167**, 054501.
43. L. Q. Wang, M. Bellini, H. A. Miller and J. R. Varcoe, *J Mater Chem A*, 2018, **6**, 15404-15412.
44. D. Li, E. J. Park, W. Zhu, Q. Shi, Y. Zhou, H. Tian, Y, Lin, A. Serov, B. Zulevi E. D. Baca, C. Fujimoto, H. T. Chung, Y. S. Kim, *Nature Energy*, 2020, **5**, 378-385.
45. M. R. Hibbs, *J Polym Sci Part B-Polym Phys*, 2013, **51**, 1736-1742.
46. S. Maurya, C. H. Fujimoto, M. R. Hibbs, C. N. Vilarrubia and Y. S. Kim, *Chem Mater*, 2018, **30**, 2188-2192.

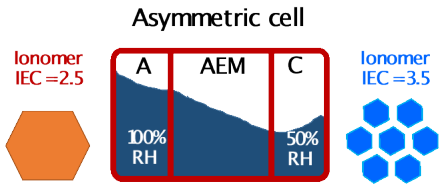

An asymmetric anion exchange membrane fuel cell enables high performance and operational durability under low RH conditions